JOURNAL OF AIRCRAFT
Vol. 43, No. 1, January–February 2006

Aircraft Ice Accretion Prediction Based on Neural Networks

E. Ogretim,* W. Huebsch,† and A. Shinn‡
West Virginia University, Morgantown, West Virginia 26506-6106

Many experimental research efforts in the past two decades have revealed that the complete picture of aircraft ice accretion has many components, resulting in a complex physical structure. Although overwhelmingly complex, the icing phenomenon needs to be understood because of its impact on aircraft performance and safety. This requires a detailed knowledge of ice accretion physics, subsequent flow over the aircraft, and the resulting modified aircraft performance. Experimental and numerical studies to address these issues have their own advantages, disadvantages, and limitations, which further limit the analysis of the icing phenomena. The motivation behind this study is the belief that complex phenomena in nature have an orderly structure on the large scale. Based on this premise, it is thought that icing phenomena also have orderly, albeit nonlinear, behavior that can be modeled by neural networks, which have a proven capability for modeling nonlinear systems. The methodology developed in the present study incorporates the Fourier series expansion of an ice shape following a conformal mapping, which suppresses the effect of airfoil geometry, and then utilizes neural networks to model the Fourier coefficients and the downstream extent of the ice shape. The neural network can be trained to make ice accretion predictions, given a set of data including the flight and atmospheric conditions, along with the Fourier coefficients and the extent of the resulting ice shape. The neural network also provides statistical output of the relative significance of the input parameters in the training. The preliminary results show that the proposed method has reasonable capabilities and has merit for further investment, because it can be coupled with other systems to create advanced computational ice accretion models and ice protection systems.

Nomenclature

a_i, b_i	=	coefficients of the cosine and sine functions of the Fourier series expansion, respectively
f	=	actual perturbation geometry from the parabola surface
$\tilde{f}$	=	approximated perturbation geometry
LWC	=	liquid water content of oncoming air in grams per cubic meter
M	=	number of Fourier terms for the truncated Fourier series expansion
MVD	=	median volumetric diameter in micrometers
N	=	number of data points of the actual ice geometry
T_∞	=	static temperature in the oncoming air in kelvin
V_∞	=	free stream velocity in meters per second
x–y	=	data coordinates of the experimental ice shape
x'–y'	=	ice shape coordinates nondimensionalized by the leading-edge radius (LER) of the airfoil
ξ–η	=	coordinates of the ice shape in the transformed plane
ξ'–η'	=	coordinates of the ice shape after separation of perturbation geometry

I. Introduction

AIRCRAFT icing has been an area of active research since the advent of high speed–high altitude flight around the time of World War II. Because of the lack of theoretical predictions for the problem, experimental studies were the main foundation of research on aircraft icing and development of ice protection systems. The Messinger model[1] was the first successful attempt to model ice accretion. This model related the accretion to the impingement of supercooled droplets onto the aircraft surface. It proposed a thin water film around the ice surface, which was fed by oncoming droplets and was responsible for further growth of ice to downstream points. This method proved successful for rime ice accretion, although it had problems for glaze ice accretion.

A follow-up study by Olsen and Walker[2] included high-speed camera pictures and movies of the ice accretion process. These clearly showed that the water film, which was assumed to cover the entire ice surface, is absent other than at some initial moments of the accretion process. Instead, according to their observations the ice growth over the surface was due to water bead formation and growth; therefore, they proposed changing the Messinger model.

The motivation for improvement of the Messinger model was not only interest in the physics, but also aircraft accidents related to ice accretion. The industry needed robust models to have flight safety and high performance even in severe weather conditions. This required better understanding of ice formation in various weather conditions, because ice protection systems relied on these results.

Following in these footsteps, studies have been conducted to better understand ice accretion phenomena, both numerically and experimentally. LWC and temperature effects on glaze ice formation,[3] effects of variable LWC in modeling variable icing cloud conditions,[4] mixed phase water content effects on the final ice shape,[5,6] surface water film instabilities,[7] and droplet impact effects on the surface water film[8] are a few of the many studies that are being performed in the effort to improve the understanding of icing physics.

The LEWICE[9] code based on the Messinger model, developed by the NASA Glenn Research Center, is one of the widely used ice accretion prediction codes. Within the LEWICE code, the icing model is coupled with other flight conditions, such as angle of attack, LWC, droplet size distribution, flight speed, and temperature and pressure at the flight altitude. LEWICE has also been subject to further development following recent findings that focus on physical phenomena, such as water film dynamics, droplet growth, droplet trajectories, heat transfer coefficient variation, and boundary layer–ice roughness interaction.[10] As a result of these studies, the performance of the LEWICE code rose to a reliable level for many icing scenarios.

Presented as Paper 2005-1245 at the AIAA 43rd Aerospace Sciences Meeting and Exhibit, Reno, NV, 10–13 January 2005; received 22 February 2005; revision received 19 May 2005; accepted for publication 21 May 2005.

*Graduate Research Assistant, Mechanical and Aerospace Engineering Department. Student Member AIAA.

†Assistant Professor, Mechanical and Aerospace Engineering Department. Member AIAA.

‡Undergraduate Research Assistant, Mechanical and Aerospace Engineering Department. Student Member AIAA.

This achieved level of ice accretion prediction was due not only to better understanding of the complex physics underlying aircraft icing, but also to better computational resources, which make possible implementation of the icing models under actual in-flight conditions. Numerical analysis of the flowfield requires a fine grid to resolve the flow details. However, flow over surfaces with ice accretion is one of the most difficult phenomena to work on, due to problems associated with grid generation over the complex geometry. Several approaches have been attempted to address orthogonality issues and to develop a quality grid. These attempts include creating multiple grid-blocks,[11] use of conformal mapping coupled with a Prandtl transposition,[12] and ice shape smoothing.[13] Another part of the grid generation problem is ice shape representation that avoids errors introduced by defects in shape modeling. The ice shape representation is also essential for the automation of grid generation. Therefore, it has been addressed by various methods, such as the use of curve fits based on control-points,[14] use of a weight function,[15] and use of Fourier series expansion.[16,17]

In terms of new methodologies for ice shape prediction, neural networks are a promising technology because of their ability to be trained and used for automation of systems that involve nonlinear dynamics. Because of this proven capability, neural networks have been applied in both aerodynamics and icing research. Some examples of this application include wake control, pressure probe calibration,[18] in-flight icing sensor device based on changes in performance coefficients,[19] and aircraft icing weather prediction.[20] The present study proposes a novel ice accretion prediction method based on Fourier expansions and the training of a neural network. The neural network learns experimental ice shape data in the form of Fourier coefficients that describe the geometry. The achieved level of learning is expressed as functions of atmospheric and flight conditions. The ice shape data set used in this study consists of two-dimensional experimental ice shapes taken at the midspan of a wing with a NACA 0012 airfoil. This data was originally generated at the NASA Icing Research Tunnel at NASA Glenn and was obtained for this study via the LEWICE validation report.[21] Since the neural network outputs the subroutine used in its prediction, it is possible to implement the developed ice accretion training in various applications. Some potential uses for this novel predictor include the following:

1) Real-time ice accretion prediction.

2) Preconditioner for ice accretion codes.

3) Rapid design tool.

4) Ice accretion predictor for computational fluid dynamics codes that solve the flowfield around the ice-accreted wing.

5) Help the estimating degradation of the aircraft performance when coupled with other software.

6) Ice protection mechanism trigger.

7) Work in parallel with LEWICE for aircraft certification in icing conditions.

The first part of the study uses the method developed by Ogretim and Huebsch[17] in order to obtain the Fourier coefficients that define the two-dimensional ice shape geometry in terms of sine and cosine terms. This part requires the experimental ice shape data points as the input and is repeated for multiple ice shapes for both rime ice and glaze ice. Although the number of Fourier terms can be optimized for better agreement between the experimental ice shape and its Fourier-regenerated ice shape, the neural network side of the study requires the number of Fourier terms to be kept as low as possible to achieve better training/prediction performance. Therefore, a preliminary study was done to determine an optimum number of Fourier terms for use with the neural network.

The second part of the study is the neural network training for ice accretion prediction. The input parameters for this part of the study are the atmospheric and flight conditions (LWC, MVD, static temperature, accretion time, and flight speed). The corresponding outputs for each ice shape are the Fourier coefficients that define the ice shape and its extent on the airfoil surface. The software package used for training purposes was NEUROSHELL 2, developed by Ward Systems, Inc. For the entire experimental data set, three separate trainings were performed using the neural network software: one for the sine terms, one for the cosine terms, and one for the downstream extent of the ice shape. After an acceptable level of training was obtained for all three networks, the respective trained networks were used to predict the sine-cosine terms and the ice extent for different icing conditions that the network has never seen. Preliminary results show a promising level of success in final ice shape prediction.

In comparing the ice shapes (experimental or predicted), a common ground is necessary to express the ice accretion quantitatively[16,22,23] and compare it with results of other researchers. To express the accuracy of the predictions quantitatively, an error analysis method containing various components is needed. For the present study, a new error analysis method was developed by the authors, called cumulative shape error. Some results are presented based on this analysis; however, for a more complete quantitative picture, the authors believe that there is a need for comparison of multiple parameters such as accreted ice amount, extent of the ice, accuracy of the bulk ice shape, and accuracy on the level of the smaller-scale roughness of the ice shape.

II. Formulation and Methodology

A. Ice Shape Fourier Coefficients

The first part of this methodology uses a technique that reduces experimental ice shape geometry to its Fourier coefficients. Because the geometric basis for this work stems from the study of Huebsch and Rothmayer,[12] the same coordinate transformations are used. The geometric meaning of these transformations is as follows: the ice shape on the airfoil leading edge is modeled as a perturbation geometry over a parabola, which resembles the airfoil leading edge; the perturbation geometry and the parabola itself are passed through conformal mapping, after which the parabola becomes a straight line and the ice roughness becomes perturbations to this straight line. These transformations are outlined below with the relevant formulae and explanation (see Ref. 17 for more details).

1) NACA 0012 airfoil is selected as the base airfoil where ice accretion takes place. The original coordinate data in the x–y plane is rescaled based on the leading-edge radius (LER) to coincide with the parabola leading-edge. The rescaling transforms the data to the x'–y' plane:

$$x' = (x/c)/(\text{ler}/c) - 0.5, \qquad y' = (y/c)/(\text{ler}/c) \tag{1}$$

An example of ice accretion on the NACA 0012 leading edge after this rescaling can be seen in Fig. 1.

2) The surface roughness (e.g., ice roughness) is introduced as perturbations to the parabola leading-edge to simulate the actual airfoil geometry with ice (Fig. 2).

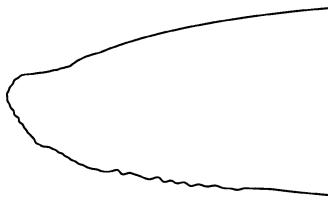

Fig. 1 NACA 0012 leading-edge and the experimental ice shape in the x'–y' plane.

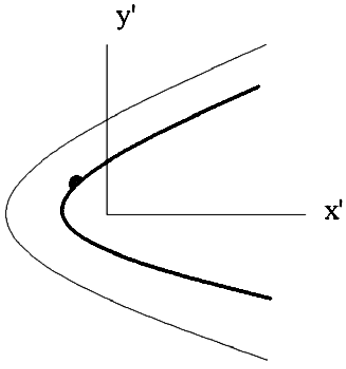

Fig. 2 Base parabola and an example perturbation in the x'–y' plane.

3) Transformation from the scaled physical plane (x'–y') to the (ξ'–η') plane using the conformal mapping

$$x' = (\xi'^2 - \eta'^2)/2, \qquad y' = \xi'\eta' \tag{2}$$

The result of this transformation is shown pictorially in Fig. 3. The base surface, which is a parabola in the x'–y' plane, becomes a straight line in the new ξ'–η' plane. The corresponding perturbations (ice roughness) on that parabola become perturbations to this straight line.

4) Separate the roughness geometry from the base surface, making use of the Prandtl transposition

$$\xi' = \xi, \qquad \eta' = \eta + f(\xi) \tag{3}$$

where $f(\xi)$ is a single-valued expression representing the shape of the perturbation geometry (Fig. 4).

5) Use a Fourier series approximation to obtain an analytical expression for the roughness geometry.[17] The typical ice roughness resembles a nonperiodic complex signal (Fig. 4), which can be expressed in terms of sine and cosine terms using a Fourier series expansion. The formulae to obtain the relevant Fourier coefficients are

$$a_i = \frac{2}{(\xi_N - \xi_1)} \int_{\xi_1}^{\xi_N} f(\xi) \cos\left(\frac{2\pi i \xi}{(\xi_N - \xi_1)}\right) \mathrm{d}\xi$$

$$\text{where} \quad i = 0, 1, 2, \ldots \tag{4}$$

$$b_i = \frac{2}{(\xi_N - \xi_1)} \int_{\xi_1}^{\xi_N} f(\xi) \sin\left(\frac{2\pi i \xi}{(\xi_N - \xi_1)}\right) \mathrm{d}\xi$$

$$\text{where} \quad i = 1, 2, 3, \ldots \tag{5}$$

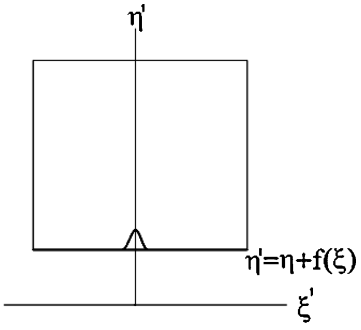

Fig. 3 Base parabola and an example perturbation in the transformed plane.

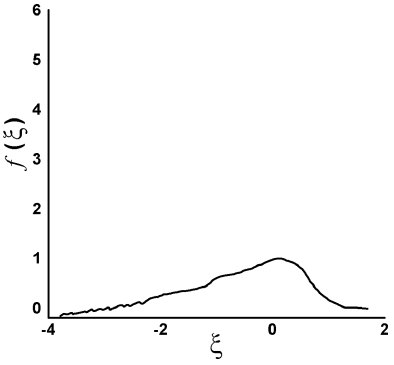

Fig. 4 Ice shape as perturbation in the transformed plane.

where ξ_1 and ξ_N are the first and the last points, respectively, a_i are the coefficients of the cosine terms, b_i are the coefficients of the sine terms, and $f(\xi)$ is the transformed experimental ice perturbation data.

The a_i and b_i coefficients are used to regenerate the original geometry through the following formula:

$$\tilde{f}(\xi) = \frac{a_o}{2} + \sum_{i=1}^{M} \left[a_i \cos\left(\frac{2\pi i \xi}{\xi_N - \xi_1}\right) + b_i \sin\left(\frac{2\pi i \xi}{\xi_N - \xi_1}\right) \right] \tag{6}$$

where $\tilde{f}(\xi)$ is the analytic roughness expression regenerated by the sine and cosine terms and M is the number of Fourier terms that are used to express the original shape. Although in theory M is infinite, for practical purposes M is truncated to 20 (hence 20 sine and 20 cosine terms) as a result of a parametric study to determine an optimum number of Fourier terms to express the ice shapes and improve the neural net training. Steps 1 through 5 are applied to numerous experimental rime and glaze ice shapes to yield their corresponding Fourier coefficients.

An important point to note is the use of SMAGGICE[14] for ice shape smoothing and/or point modification when necessary. The primary reason is that the Fourier expansion requires a single-valued data set. The experimental ice shapes may result in multivalued functions at certain locations when transformed into the ξ'–η' plane. In such a case, the Fourier series produces an approximation that has erratic behavior. It is desired therefore that the data represent a single-valued curve to achieve a better approximation to the original curve. By proper smoothing of the required regions in the ice shape by SMAGGICE, this condition is met. It should also be noted that this approach with SMAGGICE was undertaken with great care to preserve the large scale characteristics of the original ice shape.

B. Neural Network

The second part of this study made use of neural networks for ice accretion prediction. An input file is needed to train the network. This file includes the atmospheric and flight conditions of the ice accretion test and the Fourier coefficients and the extent of the corresponding ice shapes. During the training process, the network learns the Fourier coefficients of an ice shape as a function of the corresponding atmospheric and flight conditions. In other words, ice shape Fourier coefficients = function (V_∞, T_∞, LWC, MVD, spray time), where spray time is the time the airfoil is exposed to the spray of water, measured in minutes.

The Fourier model for the ice shape makes use of a large number of coefficients (upper and lower extent of ice; cosine coefficients, and sine coefficients) compared to the number of inputs. This is an undesirable condition for the neural network performance because it increases the time to train the neural net and decreases the accuracy of the predicted outputs. Therefore, separating the outputs into three different training sets (extent, cosine coefficients, and sine coefficients) reduces the number of corresponding outputs for a single training. Once the three trainings have converged to a reasonable error, the trained networks are used for prediction, which is introducing a set of inputs (i.e., icing conditions) that it has never seen before. Table 1 shows the icing parameters that were used to test the capabilities of the trained neural net in predicting rime and glaze ice accretions. Thus, the network predicts the Fourier coefficients and the ice extent corresponding to new inputs that generate the predicted ice shape by making use of Eq. (6).

To further improve the predictions, the experimental ice geometries are divided into their respective ice types, rime ice and glaze

Table 1 Input properties of the experimental ice accretions for neural net prediction

Ice type	IRT run number	Velocity, m/s	Static temperature, K	LWC, g/m^3	MVD, μm	Spray time, min
Rime	July 1996 20736	102.8	256.49	0.34	20	11.5
Rime	June 1991 27636	58.1	256.19	1.30	20	8
Glaze	July 1996 21236	102.8	262.04	0.44	30	8.75
Glaze	July 1996 21336	102.8	262.04	0.48	40	8

ice, and separate training is done for each group. This separation of ice types was performed in a qualitative manner, where the two-dimensional ice cross sections were observed and classified as either rime or glaze based upon well-known characteristics unique to each type. For example, horns and excessive ice roughness implied a glaze ice shape, whereas smooth large-scale geometry denoted a rime ice shape.

An important point to note about the performance of the neural networks is that they are advanced interpolation schemes. Therefore, they can only predict the outcomes of the conditions that fall into the range of data they have seen. Attempts to obtain a prediction that is based on conditions out of the training range will not necessarily yield reasonable results.

C. Error Analysis

To measure the success of this approach, it was apparent that a method was needed to quantitatively compare the predicted ice shapes against the experimental and LEWICE predicted ice shapes. One of the first ideas attempted was finding the two-dimensional cross-sectional area bounded by the experimental ice accretion curve and the airfoil surface, along with the area bounded by the prediction curve and the airfoil surface. Then, the difference between the prediction and the experiment could be used as a measure of the prediction error; however, two geometrically dissimilar two-dimensional objects could have the same area (e.g., Fig. 5). So although area comparison would be appropriate for ice mass error, it would not tell how well the predicted shape matched the experimental one. For this purpose, aside from the ice cross-sectional area error, a specialized error calculation was developed, which makes use of the absolute value of the local relative difference between the experiment and the prediction. The use of the absolute value of each local error avoids the canceling of a positive error by a negative one elsewhere. In the present work, the developed method utilizes the ξ–η plane representation of the ice shapes, and the error is computed by using the perturbation value, f, which is representative of the ice thickness. The following derivation for the new error analysis method, termed cumulative shape error, is depicted in Fig. 5 to provide better understanding. The absolute value of the local relative error is weighted by the area of the local rectangular element of the ice shape and summed up over the entire ice extent. The result of this summation is divided by the experimental ice area to give an area-weighted average error. The result is given as

$$\text{error} = \frac{\sum_{i=1}^{N} \left(\left| f_{e_i} - f_{p_i} \right| / \left| f_{e_i} \right| \right) \left(\left| f_{e_i} \right| \Delta\xi_i \right)}{\sum_{i=1}^{N} \left| f_{e_i} \right| \Delta\xi_i}$$

$$= \frac{\sum |i\text{th relative error}||i\text{th experimental area}|}{\text{total experimental ice area}} \tag{7}$$

where the subscript e denotes the experimental ice thickness and the subscript p denotes the predicted ice thickness, N is the total number of data points, $|f_{e_i} - f_{p_i}|/|f_{e_i}|$ is the true relative error of the local predicted thickness, and $|f_{e_i}|\Delta\xi_i$ is the absolute area of the ith rectangular element for the experimental ice shape. Because this error is an area-weighted average error, the computed error in regions of small ice thickness does not contribute as much to the overall error as the regions of large ice thickness. With this formulation, Eq. (7) provides a way to compute a prediction error that depends more on the thicker sections of the ice rather than the small-scale ice at the downstream locations.

One difficulty is that this formulation experiences division by zero at the points where there is a finite ice thickness prediction but a zero experimental ice thickness, though some algebraic manipulation is enough to remove this singularity. A more useful and fail-safe version can be achieved by canceling out $|f_{e_i}|$ and reducing the numerator to obtain Eq. (8). After this cancellation, the term in the numerator is equal to the differential area between the experimental and the predicted ice shapes. As a result, it is seen that an area-weighted true relative error is equal to the ratio of the area between the prediction and the experiment to the experimental ice area. Note that this form of the area comparison is not the same as total ice shape area comparison, because at every location the absolute value of the difference is used so that a positive error is not compensated for by a negative error elsewhere:

$$\text{error} = \frac{\sum_{i=1}^{N} \left| f_{e_i} - f_{p_i} \right| \Delta\xi_i}{\sum_{i=1}^{N} \left| f_{e_i} \right| \Delta\xi_i} = \frac{\text{total area of error region}}{\text{total experimental ice area}} \tag{8}$$

III. Results and Discussion

As a preliminary study, three neural network architectures were compared to ascertain which one could provide the best ice shape prediction. These include 1) a ward back-propagation network, 2) a general regression neural network (GRNN), and 3) a standard back-propagation network. Each of these networks was used to predict both rime ice and glaze ice using a set of 10, 20, and 30 Fourier terms. From the results of this preliminary study, it was found that having 20 Fourier terms (20 cosine, 20 sine) is the near-optimum choice for yielding both a good approximation to the ice shape and a good neural net training and prediction. The second significant finding from the preliminary study is that the optimum architecture (of the types tested) is the GRNN for rime ice prediction and the Ward net for glaze ice prediction.

An appealing aspect of the neural networks is that they output the relative significance of the input parameters in terms of the prediction. For backpropagation networks, this is represented by the contribution factor—a dimensionless number that is a rough measure

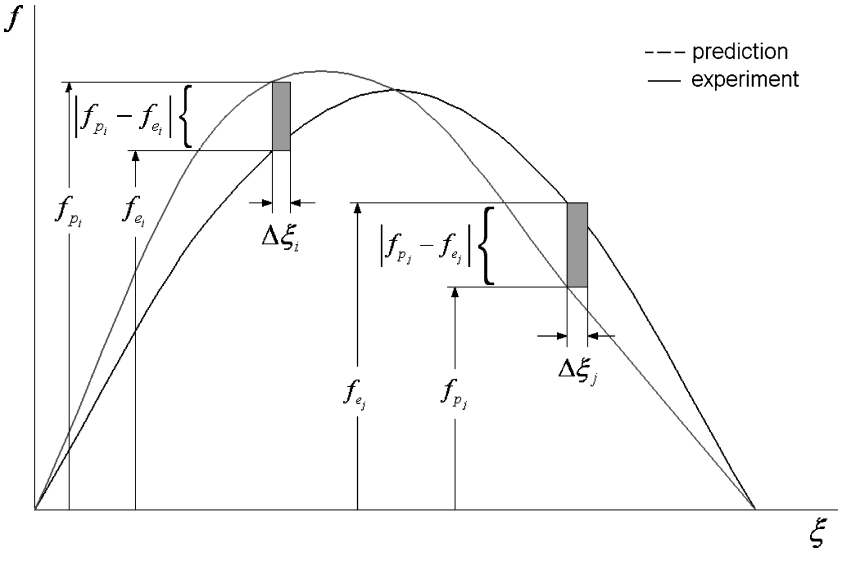

Fig. 5 Geometrical depiction for the cumulative shape error.

of the importance of an input variable in the prediction relative to the other input variables in the same network.[24] The GRNN genetic adaptive networks compute an individual smoothing factor for each input that is an analog of the contribution factor.[24] Another important point to note is that the smoothing or contribution factors are unique to the training in which they were computed and cannot be compared to any other training, even if the same network architecture is used. In the remainder of this paper, both smoothing and contribution factors will be referred to as "contribution factors" to avoid any confusion between ice shape smoothing and the smoothing factor of the GRNN.

A. Results for Neural Network Training on Rime and Glaze Ice

The use of neural networks for prediction requires a sufficient level of training (or learning) of the data set provided. In each learning cycle, the network makes a prediction of each case provided in the learning set and calibrates itself with respect to the experimental originals. Therefore, at the end of the learning process the learned ice shape and the experimental original ice shape should be in relatively good agreement. An example of this verification is provided for each of the ice types, rime and glaze, to demonstrate the adequacy of the learning (Figs. 6 and 7). A challenge in the process of learning is that in icing experiments, different ice shapes may form under the same experimental conditions. In such cases, the neural network is expected to learn an average ice shape. Figure 6 shows a comparison of experimental rime ice shapes (all accreted under the same icing conditions) to the learned ice shape from the neural net. Note that the experimental ice shapes listed in the legend use the same naming convention as the Icing Research Tunnel (IRT) at NASA Glenn. Figure 7 shows a similar comparison for the glaze ice conditions. Both of these figures clearly show that the neural net is able to statistically converge on a shape that is an average of the ice shapes formed under the same icing tunnel conditions.

Because of the nature of the training process, the prediction results are biased toward the experimental shapes due to the nature of the training process. Therefore, the proficiency obtained by the neural network at the end of the training process cannot be adequate evidence of its capabilities for the cases that it has not seen in the training process. For this purpose, the neural network is tested for the icing conditions that it has not seen before, and the resulting ice shape predictions are compared with the experimental shapes as explained below.

B. Results for Rime Ice Using GRNN

The neural net predictions using the GRNN for two rime ice cases used in the validation of this study are shown in Fig. 8 (IRT data file July 1996 20736) and Fig. 9 (IRT data file June 1991 27636) along with the corresponding experimental ice shape and the LEWICE prediction for the same case. In Fig. 8, the neural net prediction can successfully capture the maximum ice thickness as well as its

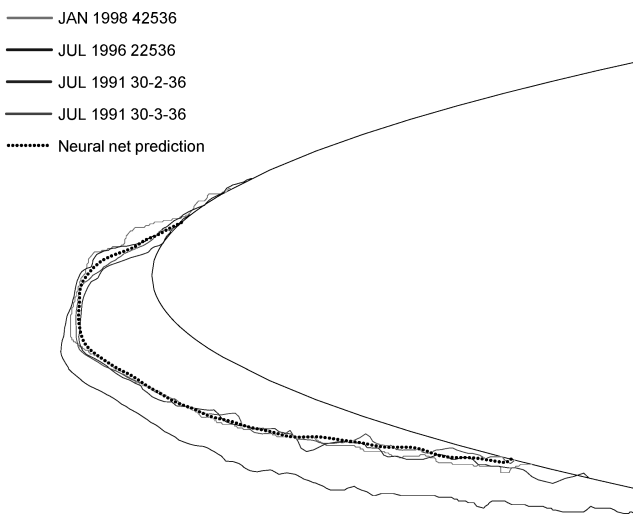

Fig. 6 Comparison of experimental rime ice shapes formed under the same conditions and ice shape learned by the neural network.

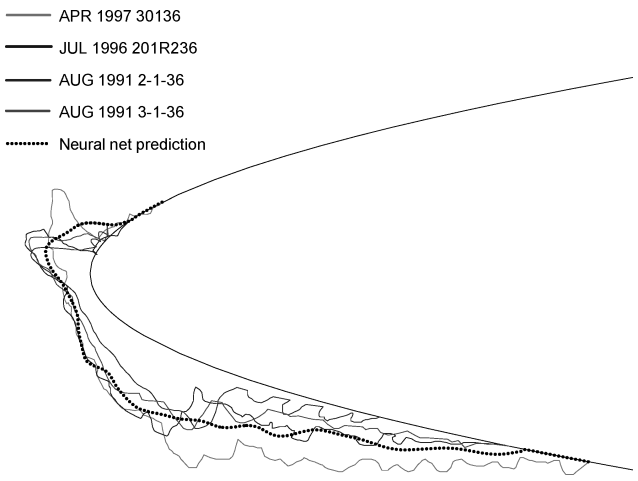

Fig. 7 Comparison of experimental glaze ice shapes formed under the same conditions and ice shape learned by the neural network.

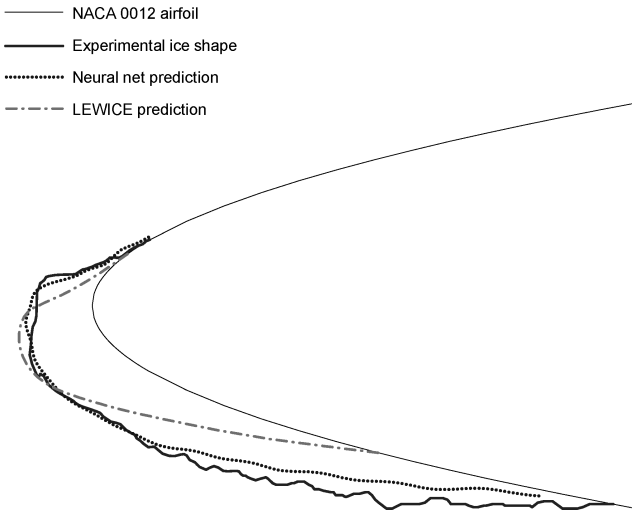

Fig. 8 Comparison of neural net and LEWICE predictions with experimental rime ice.

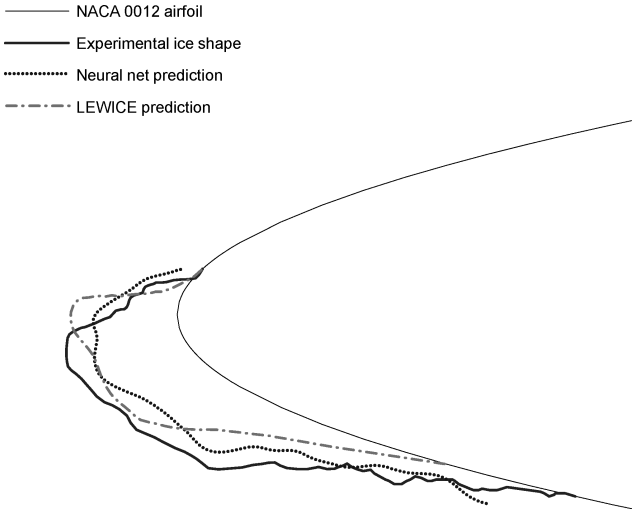

Fig. 9 Comparison of neural net and LEWICE predictions with experimental rime ice.

Table 2 Contribution factors for neural net training on sine coefficients of rime ice

Static temperature	0.08235
LWC	1.10588
MVD	2.45882
Velocity	0.05882
Spray time	0.37647

Table 3 Contribution factors for neural net training on cosine coefficients of rime ice

Static temperature	0.08235
LWC	2.75294
MVD	0.10588
Velocity	1.85882
Spray time	0.57647

Table 4 Contribution factors for neural net training on extent of rime ice

Static temperature	0
LWC	0.97647
MVD	0.21176
Velocity	1.41177
Spray time	1.49412

location and can sufficiently predict the extent of the ice on both lower and upper surfaces. Clearly, the neural net prediction is in better qualitative agreement with the experiment than the LEWICE prediction. Considering the ice shape in Fig. 9, the extent of the ice shape on the lower and upper sides and the ice surface roughness are fairly well predicted. In terms of the maximum ice thickness, the location is well predicted, but the thickness is underpredicted. As an overall evaluation, the neural networks have reasonable performance in predicting the ice thickness and its distribution over the wing surface for the rime ice cases considered. However, the second ice shape predicted by the neural network has some closure problems at the end points. A quantitative comparison of the neural net and LEWICE prediction results to the experimental results is given in the error analysis section.

The relative contributions of the input parameters for the rime ice trainings are presented in Tables 2–4. From these tables, it is concluded that MVD is the most important input parameter for the sine coefficients training, LWC is the most important factor for the cosine coefficient training, and Spray Time and Velocity are most important for the ice extent training. In all training for rime ice conditions, the contribution factor is negligible for static temperature. Based on this result, it can be concluded that the static temperature has a negligible effect on the ice growth once it drops below a critical value.

C. Results for Glaze Ice Using WARD NET

The neural net predictions using the Ward net for two glaze ice cases are shown in Figs. 10 (IRT data file July 1996 21236) and 11 (IRT data file July 1996 21336) along with the corresponding experimental ice shape and the LEWICE prediction. For the case illustrated in Fig. 10, the neural net predicts the ice thickness distribution and the extent over the lower surface very well, although the upper extent is slightly overpredicted. The maximum ice thickness and its location are also reasonably predicted, which helps preserve the hornlike shape of the ice. For the case shown in Fig. 11, the neural net predicts the lower and upper extents of the ice with about the same level of success. The ice horns and the distribution of the ice thickness over the surface are also reasonably predicted and the roughness of the experimental ice is matched to a certain level.

The relative contribution factors are presented in Tables 5–7. The tables indicate that all of the input parameters have a comparable level of importance for the training on all three components (sine-cosine-extent). For all three cases, velocity is the smallest contributor for the ice shape prediction, while Spray Time and MVD are the most significant for the sine and cosine terms.

Table 5 Sum of relative contribution factors for training on sine coefficients of glaze ice

Static temperature	3.76644
LWC	3.96987
MVD	4.18174
Velocity	3.65678
Spray time	5.42518

Table 6 Sum of relative contribution factors for training on cosine coefficients of glaze ice

Static temperature	4.60612
LWC	4.44306
MVD	4.63997
Velocity	2.70079
Spray time	4.61006

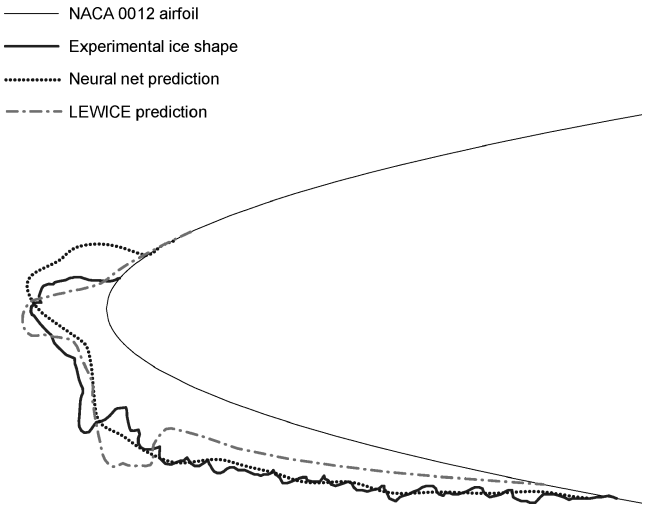

Fig. 10 Comparison of neural net and LEWICE predictions with experimental glaze ice.

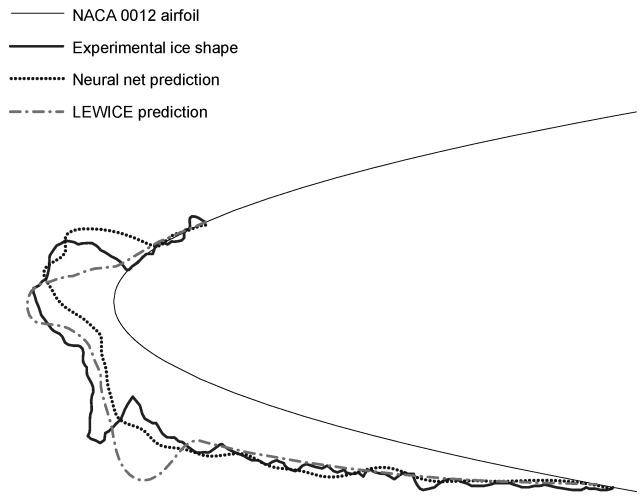

Fig. 11 Comparison of neural net and LEWICE predictions with experimental glaze ice.

D. Error Analysis

An error analysis was performed to quantify the comparison of predicted ice shapes with the experimental results. Using the transformed versions of the data in the $\xi-\eta$ plane, three different error analyses were made both for neural net predictions and LEWICE predictions for the same conditions. These analyses included 1) cumulative shape error (area-weighted error analysis) as given by Eq. (8), 2) ice cross-sectional area comparison, which is representative of ice mass error, and 3) maximum thickness height and

angle error both on the lower and upper sides of the airfoil. Note that Eq. (8), which is used for the cumulative shape error, requires exactly N data points for both the prediction and the experimental data sets, which have the same circumferential coordinate. Although for the neural net case the number of data points and their location can be chosen, the LEWICE data sets need interpolation to enable the error analysis.

Another difficulty that surfaced as a consequence of using interpolation occurred when the $\xi-\eta$ plane contained a region that was multivalued; the gap area protruding into the ice shape caused a problem in the error calculation. To remedy this, minor ice smoothing was performed. Great care was taken in conducting this minor ice smoothing to ensure that the ice shape was not significantly altered and the error analysis was still a fair comparison.

The results of the cumulative shape error analysis are given in Table 8. Here it is seen that the neural network presents a clear improvement over LEWICE in terms of the rime ice prediction, which corresponds to an average of 14% reduction in the error. For the glaze ice cases, neural net predictions have approximately the same performance as LEWICE, but LEWICE seems to be 4% more accurate in the average for the two cases tested. There is a certain level of uncertainty in the experimental data given such factors as the level of repeatability of the ice shapes and the acquisition method of the experimental ice shape data (i.e., hand-traced). It should be noted that this study represents preliminary work in the case of neural networks as an ice shape prediction tool; many avenues exist for potential improvement of the neural net prediction capabilities.

Table 7 Sum of relative contribution factors for training on extent of glaze ice

Static temperature	0.43553
LWC	0.34448
MVD	0.5831
Velocity	0.2888
Spray time	0.34809

The errors associated with the cross-sectional area of the ice shape, which is representative of the ice mass, are given in Table 9. For the glaze ice cases, both the neural net and LEWICE are on the same order of error, which is around 7% in the average compared to the experiment. As for the rime ice cases, the neural network proves to be better in predicting the ice mass, as shown by the 15% reduction of error in the average.

In addition to the cumulative shape error and the ice mass error, a maximum thickness analysis—the current method[21] of quantitative ice shape comparison—was also made. The maximum thickness height on the lower and upper surfaces and the angular difference between these maximum-thickness locations were compared with the experimental values (Table 10). For the rime ice cases, the neural net and LEWICE had different strengths, but for the angle difference between the maximum thicknesses, the neural network showed a clear improvement. For the glaze ice cases, LEWICE tended to be better at predicting the horn heights and the angular difference between these heights.

Apart from the error calculation methods discussed above, a comparison could be done based on CFD or experimental analysis of the aerodynamic performance of the predicted ice shape and the actual ice accretion. This was beyond the scope of this work, but would be a worthwhile test because the ultimate measure is how much the ice shape degrades the lift, drag, etc. For example, an ice shape prediction method could produce an ice horn at a given leading-edge location that was offset by a certain amount from the actual experimental shape. This could have a significant effect on the resulting aerodynamics, but only produce a minor error signal from the existing maximum thickness error analysis.

As a last word for the error analysis, it can be concluded that some of the errors made both by neural net and LEWICE are within the uncertainty levels involved in the wind tunnel experiments and the data reduction process following the experiments. For rime ice cases, the neural network presents a clear improvement in prediction for this preliminary study. The neural net capabilities presented in this study should be considered as a first attempt at applying this technique to ice shape prediction.

Table 8 Summary of cumulative shape errors of neural net and LEWICE predictions

Ice type	IRT run number	N.N. % error	LEWICE % error	Difference in %
Rime	July 1996 20736	12.43	35.40	22.97
Rime	June 1991 27636	22.95	27.70	4.74
Glaze	July 1996 21236	32.32	28.43	3.89
Glaze	July 1996 21336	32.46	28.23	4.23

Table 9 Summary of ice mass error of neural net and LEWICE predictions

Ice type	IRT run number	N.N. % error	LEWICE % error	Difference in %
Rime	July 1996 20736	7.22	30.39	23.16
Rime	June 1991 27636	11.58	18.55	6.96
Glaze	July 1996 21236	9.89	11.65	1.76
Glaze	July 1996 21336	2.70	4.69	1.99

Table 10 Summary of maximum thickness height and angle errors

Data file number	Prediction method	%diff. lower max. thickness	%diff. upper max. thickness	% diff. of angle diff.
IRT July 1996	LEWICE	4.7	18.2	−46
20736 (rime)	NN	−6.2	18.2	−30
IRT June 1991	LEWICE	−7.6	59.1	−84.2
27636 (rime)	NN	−19	27.3	26.3
IRT July 1996	LEWICE	17.6	13.6	6.2
21236 (glaze)	NN	−16.5	13.6	1.6
IRT July 1996	LEWICE	12	2.7	−2.6
21336 (glaze)	NN	−28	12	37.2

IV. Conclusions

A novel method for ice accretion prediction based on neural networks was developed and validated against existing experimental and LEWICE data. The new method shows promising performance, which makes it attractive due to its small computational resource requirement, fast performance, and ease of use for ice accretion predictions. It was found that the neural network approach performed very well for the rime ice accretion both in terms of the ice thickness and the ice extent. With respect to the glaze ice accretions, the neural networks need further improvement, although the current capability is comparable to that of LEWICE. It has been shown that the temperature has a negligible effect for the rime ice cases, which means that the temperature becomes irrelevant to the accretion process once it is below a critical value. On the other hand, the results showed that all of the input parameters had some level of importance in glaze ice cases.

Some limitations were found on the use of the current method. First, this method is based on the Fourier series expansion and can only produce ice shapes that are single-valued. This means that it will not predict an ice shape that folds back on itself. Second, the range of the predictions is limited to the input data range in terms of the atmospheric and flight conditions. Therefore, it will not be able to predict an ice shape accurately if its formation conditions fall beyond the values that the neural net has been trained for.

This new method has the potential to be coupled with other ice protection systems in order to increase flight safety, decrease the running cost of these systems, and make rapid ice accretion predictions making it open to further improvement and investment.

In the light of the findings of this study, the following are recommended:

1) Creation of a standardized ice shape data reduction system for quantitative comparison of icing predictions.

2) Evaluate the robustness of the neural net prediction by testing the sensitivity to unseen areas of parameter space (e.g., ice shapes on airfoil geometries not included in the training set).

3) Train neural networks with more ice accretion geometry to increase the scope of its prediction ability.

4) Use more advanced and specialized network architectures to enhance ability to learn and predict nonlinear behavior of ice geometry.

5) Extend the input parameter set to account for different variables, such as turbulence intensity, relative humidity, airfoil geometry, and angle of attack.

References

[1]Messinger, B. L., "Equilibrium Temperature of an Unheated Icing Surface as a Function of Airspeed," *Journal of the Aeronautical Sciences*, Vol. 20, No. 1, 1953, pp. 29–42.

[2]Olsen, W., and Walker, E., "Experimental Evidence for Modifying the Current Physical Model for Ice Accretion on Aircraft Surfaces," NASA TM-87184, 1986.

[3]Vargas, M., and Reshotko, E., "LWC and Temperature Effects on Ice Accretion Formation on Swept Wings at Glaze Ice Conditions," AIAA Paper 2000-0483, Jan. 2000.

[4]Koenig, G. G., Ryerson, C. C., Larsson, J., and Reehorst, A., "Effect of Variable LWC on Ice Shape in the NASA-GRC IRT," AIAA Paper 2003-904, Jan. 2003.

[5]Hallett, J., and Isaac, G., "Aircraft Icing in Glaciated and Mixed Phase Clouds," AIAA Paper 2002-0677, Jan. 2002.

[6]Al-Khalil, K., Irani, E., and Miller, D., "Mixed Phase Icing Simulation and Testing at the Cox Icing Wind Tunnel," AIAA Paper 2003-0903, Jan. 2003.

[7]Rothmayer, A. P., "On the Creation of Ice Surface Roughness by Interfacial Instabilities," AIAA Paper 2003-0972, Jan. 2003.

[8]Rothmayer, A. P., and Krakos, J. A., "Residual Droplet Impacts and Thin Film Dynamics," AIAA Paper 2004-0057, Jan. 2004.

[9]Wright, B. W., "User Manual for the NASA Glenn Ice Accretion Code LEWICE," NASA C.R. 209409, Sept. 1999.

[10]Potapczuk, M. G., "A Review of NASA Lewis' Development Plans for Computational Simulation of Aircraft Icing," AIAA Paper 99-0243, Jan. 1999.

[11]Chi, X., Zhu, B., Shih, T. I-P., Slater, J. W., Addy, H. E., and Choo, Y. K., "Computing Aerodynamic Performance of a 2D Iced Airfoil: Blocking Topology and Grid Generation," AIAA Paper 2002-0381, Jan. 2002.

[12]Huebsch, W. W., and Rothmayer, A. P., "Effects of Surface Ice Roughness on Dynamic Stall," *Journal of Aircraft*, Vol. 39, No. 6, 2002, pp. 945–953.

[13]Chung, J., Reehorst, A., Choo, Y., and Potapczuk, M., "Effect of Airfoil Ice Shape Smoothing on the Aerodynamic Performance," AIAA Paper 98-3242, July 1998.

[14]Vickerman, M. B., Choo, Y. K., Braun, D. C., Baez, M., and Gnepp, S., "SmaggIce: Surface Modeling and Grid Generation for Iced Airfoils—Phase 1 Results," AIAA Paper 2000-0235, Jan. 2000.

[15]Thompson, D. S., and Soni, B. K., "Automated Geometric Modeling and Grid Generation for Airfoils with Ice Accretions," AIAA Paper 2002-0379, Jan. 2002.

[16]Ruff, G. A., "Automated Comparison of Ice Shape Accretion Shapes," AIAA Paper 99-16491, Jan. 1999.

[17]Ogretim, E., and Huebsch, W., "A Novel Method for Automated Grid Generation of Ice Shapes for Local-Flow Analysis," *International Journal for Numerical Methods in Fluids*, Vol. 44, No. 6, 2004, pp. 579–597.

[18]Fan, H., Lu, W., Xi, G., and Wang, S., "An Improved Neural-Network-Based Calibration Method for Aerodynamic Pressure Probes," *Journal of Fluids Engineering*, Vol. 125, Jan. 2003, pp. 113–120.

[19]Melody, J. W., Pokhariyal, D., Merret, J., Basar, T., Perkins, W. R., and Bragg, M. B., "Sensor Integration for Inflight Icing Characterization Using Neural Networks," AIAA Paper 2001-0542, Jan. 2001.

[20]Pocernich, M., Wolff, C., and Fowler, T., "Statistical Models of Aircraft Icing," *17th Conference on Probability and Statistics in the Atmospheric Sciences*, American Meteorological Society, 2004.

[21]Validation Report for LEWICE 2.0, NASA CR 208690 [CD-ROM], NASA Lewis Research Center, Jan. 1999.

[22]Shin, J., "Characteristics of Surface Roughness Associated with Leading-Edge Ice Accretion," *Journal of Aircraft*, Vol. 33, No. 2, 1996, pp. 316–321.

[23]Anderson, D. N., and Shin, J., "Characterization of Ice Roughness from Simulated Icing Encounters," AIAA Paper 97-0052, Jan. 1997.

[24]NeuroShell 2 Help File Documentation, NeuroShell 2, Release 4.0, Ward Systems Group, Inc., 2003.